Anthropomorphic Robotic Arm With Integrated Elastic Joints for TCM Remedial Massage

Yuancan Huang, Jian Li, Qiang Huang, Philippe Souères

Anthropomorphic Robotic Arm With Integrated Elastic Joints for TCM Remedial Massage

Yuancan Huang[1,2], Jian Li[1], Qiang Huang[1], and Philippe Souères[2]

Abstract— **For reproducing the manipulation of TCM remedial massage and meanwhile guaranteeing safety, a 4-DOF anthropomorphic robotic arm with integrated elastic joints is developed, and a passivity-based impedance control is used. Due to the series elasticity, integrated joints may minimize large forces which occur during accidental impacts and, further, may offer more accurate and stable force control and a capacity for energy storage. Human expert's fingertip force curve in the process of massage therapy is acquired *in vivo* by a dedicated measurement device. Then, three massage techniques, pressing, kneading and plucking, are implemented by the soft arm, respectively, on torso model *in vitro* and on human body *in vivo*. Experimental results show that the developed robotic arm can effectively replicates the TCM remedial massage techniques.**

I. Introduction

In general, massage involves working and acting on the body with pressure, done manually or with mechanical aids, to enhance function, aid in the healing process, decrease muscle reflex activity, inhibit motor-neuron excitability, promote relaxation and well-being, and be usually taken as a recreational activity. Massage is, however, laborious, time-consuming, and monotonous. It is natural to expect that robots are used to free massagists from exhausting manipulation. Kume *et al*. [1] developed a massage robot with two end-effectors to implement the repetitive action of grasping on soft tissues. Jones *et al*. [2] showed that the ring and linear kneading manipulation can be reproduced by PUMA 562 robot. Koga *et al*. [3] created an oral rehabilitation robot that rubs the face along blood vessel, parotid duct, and muscular fiber, or provides stimuli around some of the maxillofacial tissues via rotational movements.

Traditional Chinese Medicine (TCM) remedial massage is a non-invasive hands-on body treatment that uses Chinese taoist and martial arts principles in an effort to bring the eight principles of TCM into balance. The practitioner may brush, knead, roll/press, and rub muscle groups, joints, sites of pain and poor circulation, or the same meridians and points used in acupuncture. Nowadays, absorbing with Western medicine ideology, TCM remedial massage has become rather advanced in treatment of many diseases, widely practiced in every levels of hospital throughout China.

Robotic arms with compliant joints, such as DLR lightweight arm [4], iCub [5], Meka compliant arm [8], Cog [9], exhibit simultaneously superiority on safety during human-robot impacts and good performance. Therefore, they are competent to reproduce the TCM remedial massage and to guarantee safety. As far as scientific research is concerned, our ultimate goal is that robot can do massage as well as human therapist. However, since massage techniques practiced by human therapist are very complicated, and fairly diverse, the blueprint for robot massage is formulated into three gradually-improved stages: anthropomorphic compliant robotic arms without wrist, with wrist, and with both wrist and dexterous hand. At initial stage, we focus on developing a high-torque integrated joint with series elasticity, whose low impedance can effectively decouple the link's inertia from the actuator's reflected inertia whenever impact occurs. Further, it offers more accurate and stable force control and the capacity for energy storage [10], [11], [12]. Then, three point-contact massage techniques without wrist movement, pressing, kneading, and plucking, are deliberately chosen in order to be realized readily by a 4-DOF anthropomorphic robotic arm, bestowed with the characteristics of intrinsic passive compliance, light-weight and modularization. A passivity-based impedance control [13], [14] is implemented for both free and contact motions in robot massage.

The remainder of this paper is organized as follows: Section II presents design on integrated elastic joint and 4-DOF anthropomorphic soft arm. Three massage techniques, pressing, kneading and plucking, are simplified to meet the requirements by robot implementation, and the massage motion planning method is introduced in Section III. Passivity-based impedance control for robot massage as well as its passivity analysis are presented in Section IV. Next, the human expert's fingertip force curve in the process of massage therapy is measured *in vivo* by a dedicated measurement device in Section V. The massage techniques are implemented by the 4-DOF anthropomorphic robotic arm in the manner similar to that of human expert on the torso model *in vitro* and on human body *in vivo*, respectively. Finally, Section VI draws a conclusion and envisions further works on robot massage.

*This work was supported by the National Natural Sciences Foundation of China under Grant 61075080 and by the National Key Technology R&D Program of the Twelfth Five-Year Plan under Grant 2012BAI25B01.

[1]Yuancan Huang, Jian Li, and Qiang Huang are all with the Bionic Robot and System Key Laboratory, School of Mechatronical Engineering, Beijing Institute of Technology, 5 South Zhongguncun Street, Haidian District, 100081 Beijing, China yuancanhuang@bit.edu.cn.

[2]Yuancan Huang and Philippe Souères are with CNRS, LAAS, 7 avenue du colonel Roche, F-31400 Toulouse, France, and Univ de Toulouse, LAAS, F-31400 Toulouse, France yuancan.huang@laas.fr.

II. Integrated Elastic Joint and 4-DOF Anthropomorphic Robotic Arm

Human arm can be modeled as a 7-DOF fully-rotational-joint redundant robotic arm, which has three mutually orthogonal rotational joints at the shoulder that can rotate in any direction, a single rotational joint at the elbow, and three rotational joints at the wrist. Since our goal in this paper is to build a robotic arm mimicking the massage techniques scarcely with wrist movements, a 4-DOF fully-rotational-joint nonredundant configuration is enough for this requirement, but it can be extendable. In robotic arm, elastic joints, which are essentially springs in series with stiff actuators, are used to provide fixed passive compliance for safety of human-robot impact, and their apparent compliance can be actively changed by control. On the other hand, the spring's elongation is a measurement of applied torque, thus torque feedback control is easy to implement in the joint level. Circuit boards and mechanical components are incorporated into a compact joint module, and robotic arm is built with modularized method. Modularized design contributes to many merits, *e.g.*, high dependability, readily used and maintained, cost reduction, and easily manufactured in bulk.

A. Integrated Elastic Joint

As shown in Fig. 1, integrated elastic joint mainly contains three components: actuation unit, Elastic connector, and control and drive circuits.

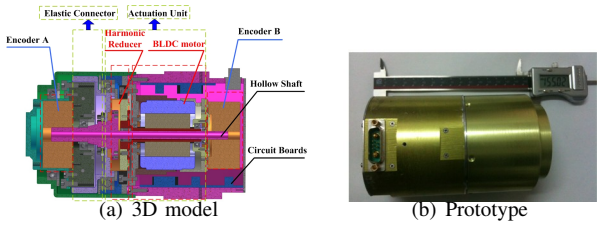

(a) 3D model (b) Prototype

Fig. 1: Integrated elastic joint

1) Actuation Unit: Actuation unit is composed of Kollmorgen frameless BLDC motor RBE1213 and HD zero-backlash harmonic reducer CSD 25. For the sake of compactness, a hollow shaft around the joint axis crosses over the central orifice of rotor and the wave generator, through which photoelectric encoder A is wired to the circuit board on the opposite side. Encoder A measures the rotation of elastic connector relative to the flex spline, and Encoder B the rotation of the flex spline relative to the joint frame (see Fig. 1).

2) Elastic Connector: Elastic connector connecting the actuated unit to the joint output shaft is crucial. It not only decomposes mechanically the rigid actuation unit from the joint output shaft, but also reflects the output torque by the springs' deflections. As illustrated in Fig. 2, 4 input sectoral blocks and 8 linear springs are evenly positioned along a circular circumference. Analogous to derivation in [5], [6], relation between the rotational joint torque T and the deflected angle of the output spoke θ_s is given as follows:

$$T = 4K_S\left(R^2 + \frac{r_S^2}{3}\right)\sin(2\theta_S),$$

where K_S is the linear spring axial stiffness, R the length of the spoke arm, and r_S the spring external radius.

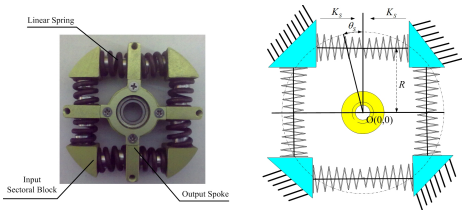

Fig. 2: Elastic connector

3) Control and Drive Circuits: In order to eliminate electromagnetic interferences, control and drive circuit modules are separated physically on two PCBs, shown as Fig.3. Considering miniaturization and reliability, a FPGA-centered control circuit is adopted. Control algorithms, CAN communication protocol, and all sensor's information are implemented, acquired and processed by only one medium-scale Altera FPGA chip, model EP2C35F484C7, with thirty-five thousands of logic elements. Drive circuit has six N-channel power MOSFETs for 3-phase full-bridge inverter.

Generally, careful design of power supply is a significant prerequisite for electric systems. Two important issues are considered here: Isolation and power density. From our debugging experiences, the motor driver is one of the principal disturbance sources responsible for malfunction of control circuit. Thus, a power supply module with isolated transformer is used to separate each other the power supplies of the controller and the driver. In addition, the peak power requirement may be extremely huge while several joints work simultaneously. A bank of supercapacitors, which are means of storing energy like battery, is employed to provide high peak power and to improve power density.

Since the assembly space is narrow and airtight, particular attention has been paid to heat dissipation. A thermally conductive silicon rubber pad is used to press the six power MOSFETs tightly against the shell of the joint keeping them from over-heating.

4) Specifications: Technical data of integrated elastic joint are listed in Table I.

B. 4-DOF Anthropomorphic Robotic Arm

A well-designed robot structure has a lower weight-to-payload ratio, higher stiffness and natural frequencies, and larger workspace. In order to achieve these targets, the following design rules should be obeyed entirely or, at least, partially [7]:

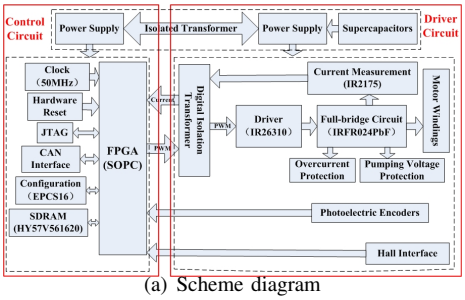

(a) Scheme diagram

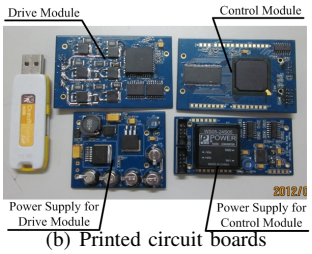

(b) Printed circuit boards

Fig. 3: Control and drive circuits

TABLE I: Technical data of integrated elastic joint

Items	Specifications
Weight	2.1 kg
Size	Φ90×55 mm
Nominal output torque	70 Nm
Max. output torque	160 Nm
Torque resolution	0.336 Nm
Rotational stiffness	519.4 Nm/rad
Nominal voltage	24 V
Max. current	8.8 A

- For substantially improving the workspace, the arm links should be designed to be of the same length and the wrist to be as short as possible,.
- For reducing the torques required to counteract gravity forces, the linkage masses are reduced and/or the locations of their center of gravity points are shifted closer to joint pivots.
- For enhancing responsiveness and overall performance of the arms as well as reducing the influence of coupling and nonlinearity and the inertias of motors, an effective way is to reduce masses and moments of inertia of links.
- For higher stiffness of the arm links, a beam with thin-walled square cross sections would be preferred to the hollow round beam.

In Fig. 4, a four-rotational-joint robot arm with the ceramic massage head is developed with the following properties:

- The consecutive joint axes intersect, and the intersecting points are all collinear. Hence, the common perpendicular has a length of zero and is located at the intersection point.
- All of the robot arm links are perforated with rectangular holes for weight-saving so as to improve the dynamics.
- The two links, connecting the shoulder with the elbow and the elbow with the massage head, are of the equal length.
- The links with thin-walled square cross section is used, and a concave protrude is designed to dwell the joint, thereby rendering the center of mass close to the intersection point.

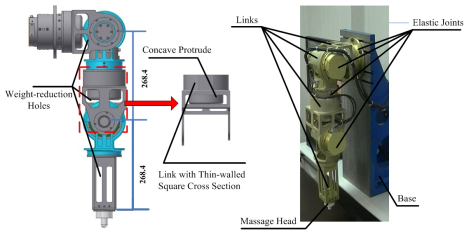

Fig. 4: 4-DOF anthropomorphic robotic arm

This robot arm is 15.2kg in weight and 809.4mm in length. Its output force is up to 14.5kg, and hence the load to weight ratio is approximately 0.95.

III. Massage Motion Planning

A. Massage Technique Description

Three types of massage techniques, which are reasonably simplified to be implemented by the robotic arm, are delineated as follows:

- **Pressing:** The robotic arm moves over a designated point (usually an acupuncture point), slowly goes downward and contacts to the body, then increases pressure gradually until a prescribed force is achieved and stays motionless for a few minutes with the force. Finally, moves up and begins a new cycle.
- **Kneading:** The robotic arm moves over a designated point (usually an acupuncture point), slowly goes downward and contacts to the body, then moves periodically in the pattern of tiny circle around the designated point with fixed downward force.
- **Plucking:** The robotic arm moves over a designated point (usually an acupuncture point), slowly goes downward and contacts to the body, then pushes rectilinearly along the body with fixed downward force. When another designated point is reached, moves back and starts a new run.

B. Motion Planning

1) Forward Kinematics: A set of link frames is assigned in Fig.5, and Denavit-Hartenberg parameters are defined according the following convention:

1) The link offset d_i is the algebraic distance along axis z_{i-1} to the point where the common perpendicular to axis z_i is located.
2) The link length a_i is the length of the common perpendicular axes z_{i-1} and z_i, *i.e.*, the parameter a_i is equal to the shortest distance between consecutive joint axes z_{i-1} and z_i.

TABLE II: Denavit-Hartenberg parameters of 4-DOF anthropomorphic robotic arm

i	d_i	a_i	α_i	θ_i
1	d_1	0	0	θ_1
2	0	0	90°	θ_2+90°
3	0	0	90°	θ_3
4	$-d_4$	0	90°	θ_4+90°
5	0	$-a_5$	0	0

3) The link angle θ_i is the angle around z_i that x_i makes with x_i, and counterclockwise is positive.
4) The link twist α_i is the angle around x_{i-1} that z_{i-1} makes with z_i, and counterclockwise is conventionally positive.

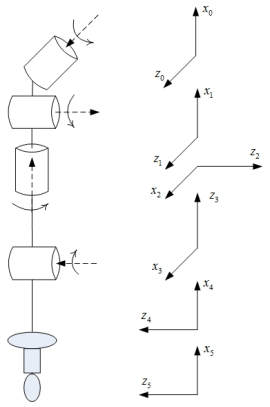

Fig. 5: Definition of link frames

Denavit-Hartenberg parameters of 4-DOF anthropomorphic robotic arm are given in Table II. In this convention, the homogeneous transformation matrix from frame $i-1$ to frame i is written as

$$\begin{aligned} {}^{i-1}_{i}A &= Trans(z_{i-1},d_i)Rot(x_{i-1},\alpha_i)Rot(z_i,\theta_i)Trans(x_i,a_i) \\ &= \begin{bmatrix} c_i & -s_i & 0 & c_i a_i \\ \gamma_i s_i & \gamma_i c_i & -\sigma_i & \gamma_i s_i a_i \\ \sigma_i s_i & \sigma_i c_i & \gamma_i & \sigma_i s_i a_i + d_i \\ 0 & 0 & 0 & 1 \end{bmatrix}, \end{aligned}$$

where, for simplicity of notation, $c_i = cos\theta_i$, $s_i = sin\theta_i$, $\gamma_i = cos\alpha_i$, and $\sigma_i = sin\alpha_i$.

The transformation that relates the massage head frame 5 to the base frame 0 is obtained as

$$\begin{aligned} {}^{5}_{0}A &= {}^{1}_{0}A\,{}^{2}_{1}A\,{}^{3}_{2}A\,{}^{4}_{3}A\,{}^{5}_{4}A \\ &= \begin{bmatrix} & R & & \vdots & \boldsymbol{p} \\ \cdots & \cdots & \cdots & \vdots & \cdots \\ 0 & 0 & 0 & \vdots & 1 \end{bmatrix}, \end{aligned}$$

where $R = \{r_{ij}\}$ is a 3×3 head rotation matrix and $\boldsymbol{p} = [p_x, p_y, p_z]^T$ is a 3×1 head position vector with respect to the base, and there are

$$\begin{aligned} r_{11} &= (c_1 s_2 c_3 - s_1 s_3)s_4 + c_1 c_2 c_4, \\ r_{12} &= (c_1 s_2 c_3 - s_1 s_3)c_4 - c_1 c_2 s_4, \\ r_{13} &= -c_1 s_2 s_3 - s_1 c_3, \\ r_{21} &= (s_1 s_2 c_3 + c_1 s_3)s_4 + s_1 c_2 c_4, \\ r_{22} &= (s_1 s_2 c_3 + c_1 s_3)c_4 - s_1 c_2 s_4, \\ r_{23} &= -s_1 s_2 s_3 + c_1 c_3, \\ r_{31} &= -c_2 c_3 s_4 + s_2 c_4, \\ r_{32} &= -c_2 c_3 c_4 - s_2 s_4, \\ r_{33} &= c_2 s_3, \\ p_x &= -r_{11} a_5 - c_1 c_2 d_4, \\ p_y &= -r_{21} a_5 - s_1 c_2 d_4, \\ p_z &= -r_{31} a_5 - s_2 d_4 + d_1. \end{aligned}$$

One common representation of the head orientation is roll-pitch-yaw (RPY) angles (α,β,γ). The conversion from head rotation matrix to RPY angles is

$$\begin{aligned} \alpha &= \text{atan2}(r_{32}, r_{33}) \\ \beta &= \text{atan2}(-r_{31}, \sqrt{r_{11}^2 + r_{21}^2}) \\ \gamma &= \text{atan2}(r_{21}, r_{11}) \end{aligned}$$

where atan2 is the two-argument arc tangent function, and assume that the pitch angle β is not equal to or greater than $\pm 90^\circ$.

2) Inverse Kinematics: Given a desired position and orientation of the massage head with respect to the base, we must compute all possible sets of joint angles which could be used to attain the given position and orientation. In general, the inverse kinematics of 4-DOF robotic arms can be solved analytically by algebraic manipulation. Assume that the desired position and orientation of the massage head is represented by the 4×4 homogeneous matrix:

$$\begin{aligned} {}^{5}_{0}A &= \begin{bmatrix} r_{11} & r_{12} & r_{13} & p_x \\ r_{21} & r_{22} & r_{23} & p_y \\ r_{31} & r_{32} & r_{33} & p_z \\ 0 & 0 & 0 & 1 \end{bmatrix} \\ &= {}^{1}_{0}A(\theta_1)\,{}^{2}_{1}A(\theta_2)\,{}^{3}_{2}A(\theta_3)\,{}^{4}_{3}A(\theta_4)\,{}^{5}_{4}A(0). \end{aligned}$$

Post-multiplying both sides of the equation by $[{}^{5}_{4}A(0)]^{-1}$, we have

$${}^{1}_{0}A(\theta_1)\,{}^{2}_{1}A(\theta_2)\,{}^{3}_{2}A(\theta_3)\,{}^{4}_{3}A(\theta_4) = \begin{bmatrix} r_{11} & r_{12} & r_{13} & p'_x \\ r_{21} & r_{22} & r_{23} & p'_y \\ r_{31} & r_{32} & r_{33} & p'_z \\ 0 & 0 & 0 & 1 \end{bmatrix} \quad (1)$$

with

$$p'_x = p_x + a_5 r_{11},\ p'_y = p_y + a_5 r_{21},\ p'_z = p_z + a_5 r_{31}.$$

Equating the elements (1,1), (1,2), (2,1) and (2,2) from both sides of Eq. (1), it follows

$$\begin{cases} (c_1s_2c_3 - s_1s_3)s_4 + c_1c_2c_4 &= r_{11} \\ (c_1s_2c_3 - s_1s_3)c_4 - c_1c_2s_4 &= r_{12} \end{cases} \quad (2)$$

and

$$\begin{cases} (s_1s_2c_3 + c_1s_3)s_4 + s_1c_2c_4 &= r_{21} \\ (s_1s_2c_3 + c_1s_3)c_4 - s_1c_2s_4 &= r_{22}. \end{cases} \quad (3)$$

Simplifying (2) and (3) with simple algebraic manipulation and noting that $p'_x = -c_1c_2d_4$ and $p'_y = p'_x = -s_1c_2d_4$, we have

$$\begin{cases} r_{11}c_4 - r_{12}s_4 &= -p'_x/d_4 \\ r_{21}c_4 - r_{22}s_4 &= -p'_y/d_4. \end{cases} \quad (4)$$

Solving the equation, we get

$$\theta_4 = \text{atan2}\left(\frac{r_{21}p_x - r_{11}p_y}{r_{12}r_{21} - r_{11}r_{22}}, \frac{r_{22}p_x - r_{12}p_y}{r_{12}r_{21} - r_{11}r_{22}}\right),$$

if $r_{12}r_{21} - r_{11}r_{22} \neq 0$.

Likewise, pre-multiplying Eq.(1) by $[{}^1_0A(\theta_1)]^{-1}$ and equating the corresponding elements from both sides, if $c_2 \neq 0$, we can derive

$$\begin{aligned} \theta_2 &= \text{atan2}\left(-p'_z, \pm\sqrt{d_4^2 - (p'_z)^2}\right), \\ \theta_1 &= \text{atan2}\left(\frac{-p'_y}{c_2}, \frac{-p'_x}{c_2}\right), \\ \theta_3 &= \text{atan2}\left(\frac{r_{33}}{c_2}, \frac{-r_{31} + s_2c_4}{c_2s_4}\right). \end{aligned}$$

.

3) Point-to-Point Motion Planning: Whilst the robotic arm does massage, its surrounding may be regraded unchangeable and is normally uncluttered. Speaking in robotics terminology, its environment space may be consider as a structured, simple environment. Thereby, it is sufficient to plan massage movements in joint space. In terms of massage techniques and surrounding conditions, a sequence of anchor points is assigned *a priori*, and several via points are inserted among anchor points in need of some purpose, such as avoiding the obstacles. Then, cubic or higher-order polynomials are used to interpolate path segments between these given points satisfying position, velocity, acceleration constrains at each point and smoothness on the overall path. Taking pressing massage as an example, anchor points are set sequentially as initial position A_1, a position over contact point A_2, and a position under contact point A_3. One via point B_1 is inserted between A_1 and A_2 in order to, for example, detour an obstacle.

IV. Passivity-based Impedance Control

During robot massage process, the human body is required to keep relaxed and still as far as possible. The massage robotic arm can be considered to couple mechanically with a passive environment. On the other hand, soft tissue exhibits viscoelasticity when undergoes small displacement, rigidity when undergoes large displacement. It is a reasonable hypothesis that the robotic arm's motion is kinematically constrained, *i.e.*, the interacted environment admits representation as an admittance. According to causal analysis, the ideal robot behavior should be an impedance, which may be regarded as a dynamic generalization of a mass-spring-damper system, returning force in response to applied displacement, velocity and acceleration [17]. Therefore, if a passive impedance controller is constructed, a stable robot massage manipulation can be accomplished.

A. Dynamical Description of Robotic Arm

The joint series elasticity can be modeled as torsional springs, as illustrated in Fig. 6. Under two mild assumptions that the rotor/gear inertia is symmetric around the rotor axis of rotation and the rotors has only pure rotation with respect to an inertial frame. Amounting to neglect the terms of order at most $1/m$ where $m:1$ is the gear ratio, the dynamics of n-DOF soft arm can be simplified as [15]:

$$\begin{aligned} M(\boldsymbol{q})\ddot{\boldsymbol{q}} + C(\boldsymbol{q},\dot{\boldsymbol{q}})\dot{\boldsymbol{q}} + \boldsymbol{g}(\boldsymbol{q}) &= \tau + \tau_{ext} \\ B\ddot{\theta} + \tau &= \tau_m \\ \tau &= K(\theta - \boldsymbol{q}), \end{aligned} \quad (5)$$

where the $n \times 1$ vectors $\boldsymbol{q}$ and θ are the n link side and motor angular positions, respectively. The $n \times n$ matrix $M(\boldsymbol{q})$ is the (link side) inertia matrix and $C(\boldsymbol{q},\dot{\boldsymbol{q}})\dot{\boldsymbol{q}}$ is the centrifugal and Coriolis terms. The $n \times 1$ vector of gravity torques $\boldsymbol{g}(\boldsymbol{q})$ is given by the differential of a potential function $V_g(\boldsymbol{q})$, i.e., $\boldsymbol{g}(\boldsymbol{q}) = (\partial V_g(\boldsymbol{q})/\partial \boldsymbol{q})^T$. K and B are the n-dimensional diagonal matrices containing the joint stiffness values k_i and the rotor inertias B_i reflected to the link side as their diagonal terms. The $n \times 1$ vectors τ, τ_m and τ_{ext} represent the spring torque, the motor torque and the contact force acting from human body on robotic arm, respectively. Due to using frictionless bearings in each joint, note that the joint damping coefficients and friction torques are negligible for the sake of brevity.

Remark 4.1: In general, all massage manipulations may be modeled as either point contact or surface contact between massage head and human body. If contact dynamics may be accurately modeled, from control viewpoint, two contact modes make no difference. Unfortunately, contact dynamics is hardly modeled in real-time with satisfactory accuracy if not possible at all. A practical solution without contact dynamics modelling is suggested in the "Experimental Verification" section.

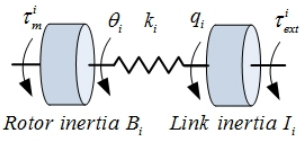

Fig. 6: Dynamic model of the i-th integrated elastic joint

As for robot dynamical model, three properties are well known:

Property 4.2: The inertia matrix $M(\boldsymbol{q})$ is symmetric and positive definite:

$$M(\boldsymbol{q}) = M^T(\boldsymbol{q}) > 0, \quad \forall \boldsymbol{q} \in R^n.$$

Property 4.3: The matrix $\dot{M}(\boldsymbol{q}) - 2C(\boldsymbol{q},\dot{\boldsymbol{q}})$ is skew symmetric:

$$\boldsymbol{y}^T(\dot{M}(\boldsymbol{q}) - 2C(\boldsymbol{q},\dot{\boldsymbol{q}}))\boldsymbol{y} = 0, \quad \forall \boldsymbol{y},\ \boldsymbol{q},\ \dot{\boldsymbol{q}} \in R^n.$$

Property 4.4: There exists a positive constant k_g such that [16]

$$k_g \geq \left\| \frac{\partial \boldsymbol{g}(\boldsymbol{q})}{\partial \boldsymbol{q}} \right\|, \quad \forall \boldsymbol{q} \in R^n.$$

B. Joint Impedance Control

Two-loop control scheme in Fig. 7 is built in each joint. The inner loop is formed by torque feedback. As for the outer loop, it may be position, force, or impedance control. From energy shaping viewpoints of state feedback [18], there are the following observations:

- The joint torque feedback loop can be regarded as shaping of motor inertia, and
- the feedback of the motor position is physically interpreted as shaping of potential energy.

With the physical interpretations, impedance control may be implemented by changing only the nature of the desired (shaped) potential energy through motor position feedback and expressing motor position in the link side angular position. Meanwhile, torque loop can be independently designed for maximal performance in terms of reducing motor inertia and friction.

Consider the i-th joint torque control in the following form:

$$\tau_m^i = \frac{B_i}{B_a^i} u_i + \left(1 - \frac{B_i}{B_a^i}\right) \tau_i, \tag{6}$$

where u_i is an intermediate control input and B_a^i is the motor apparent inertia with respect to input u_i, and $B_a^i < B_i$. This is basically a proportional torque controller with an additional fixed term, $B_i/B_a^i u_i$.

Together with the dynamics of i-th motor rotor in Eq.(5), the given torque control law leads to

$$B_a^i \ddot{\theta}_i + \tau_i = u_i, \tag{7}$$

where the ratio B_i/B_a^i (and thus the achievable bandwidth of the torque controller) only depends on the noise level of the torque sensors. Obviously, any perturbing torque acting on motor side (e.g., friction torque) is also scaled down by the factor B_i/B_a^i. The equation shows clearly that the torque controller converts the motor inertia to the apparent inertia B_a^i for the new subsystem with input u_i.

Here, we just consider the desired impedance only characterized by joint stiffness and damping coefficient not involving in inertia shaping. A choice for such outer loop controller is given by [19], [20]:

$$\begin{aligned} u_i &= -k_q^i \delta q_i - d_q^i \dot{q}_i + g_i(\boldsymbol{q}), \\ \delta q_i &= q_i - q_d^i, \end{aligned} \tag{8}$$

where q_d^i is the desired link angular position, and k_q^i and d_q^i are positive real scalars for the desired joint stiffness and damping coefficient, respectively. In essence, the outer-loop controller is exactly PD controller with gravity compensation.

If overall system is asymptotically stable, there exist the following conditions at equilibrium pair $(\theta_e, \boldsymbol{q}_e)$:

$$\begin{aligned} k_i(\theta_e^i - q_e^i) &= g_i(\boldsymbol{q}_e) - \tau_{ext}^i, \\ k_i(\theta_e^i - q_e^i) + k_q^i \delta q_i &= g_i(\boldsymbol{q}_e), \\ \delta q_i &= q_e^i - q_d^i. \end{aligned}$$

This leads to the desired joint stiffness relation $\tau_{ext}^i = k_q^i \delta q_i$.

C. Control Formulation of Robotic Arm

Putting all the outer loop controller into vector form, it follows

$$\boldsymbol{u} = -K_q \delta \boldsymbol{q} - D_q \dot{\boldsymbol{q}} + \boldsymbol{g}(\boldsymbol{q}). \tag{9}$$

The corresponding equilibrium conditions are listed as:

$$K(\theta_e - \boldsymbol{q}_e) = \boldsymbol{g}(\boldsymbol{q}_e) - \tau_{ext} \tag{10}$$

$$K(\theta_e - \boldsymbol{q}_e) + K_q \delta \boldsymbol{q} = \boldsymbol{g}(\boldsymbol{q}_e). \tag{11}$$

Similarly, we have $\tau_{ext} = K_q \delta \boldsymbol{q}$ at any equilibrium position.

Remark 4.5: Since the designed massage head is required to only exert a translational force on human body, it is unnecessary to consider rotational stiffness. Let $\boldsymbol{p}_e$ and $\boldsymbol{p}_d$ be the desired and actual Cartesian positions of the massage head with respect to a base frame. Defining $\triangle \boldsymbol{p} = \boldsymbol{p}_e - \boldsymbol{p}_d$, the translational stiffness is expressed as

$$K_p \triangle \boldsymbol{p} = \boldsymbol{F}_{ext},$$

where K_p is the 3×3 positive stiffness matrix, while $\boldsymbol{F}_{ext}$ is the force vector applied by the body on the robotic arm expressed in the base frame. Hence, there is

$$\tau_{ext} = J^T(\boldsymbol{q}) \boldsymbol{F}_{ext} = J^T(\boldsymbol{q}) K_p \triangle \boldsymbol{p},$$

where the $3 \times n$ matrix $J(\boldsymbol{q})$ is the Jacobian.

However, the control law (9) does not satisfy the required passivity condition so that the complete system cannot be ensured stable. A solution is to choose $\boldsymbol{u}$ as a function of θ and its derivative $\dot{\theta}$ only by replacing $\boldsymbol{q}$ with its stationary equivalent to $\hat{\boldsymbol{q}}(\theta)$ [13], [14], namely:

$$\boldsymbol{u} = -K_q \delta \hat{\boldsymbol{q}}(\theta) - D_q \dot{\theta} + \boldsymbol{g}(\hat{\boldsymbol{q}}(\theta)), \tag{12}$$

where $\delta \hat{\boldsymbol{q}}(\theta) = \hat{\boldsymbol{q}}(\theta) - \boldsymbol{q}_d$.

From (11), we get

$$\theta = \boldsymbol{f}(\boldsymbol{q}) = \boldsymbol{q} + K^{-1}(-K_q \delta \boldsymbol{q} + \boldsymbol{g}(\boldsymbol{q})),$$

which can be used to solve $\hat{\boldsymbol{q}}(\theta)$ from θ in the sufficiently small neighborhood of the equilibrium pair $(\theta_e, \boldsymbol{q}_e)$. Generally, the inverse function $\boldsymbol{f}^{-1}$ has not analytic expression. For a given θ, it is possible to approximate the value $\hat{\boldsymbol{q}}(\theta) = \boldsymbol{f}^{-1}(\boldsymbol{q})$ with arbitrary precision by iteration $\boldsymbol{q}_{m+1} := \theta - K^{-1}\boldsymbol{h}(\boldsymbol{q}_m)$, where $\boldsymbol{h}(\boldsymbol{q}) = -K_q \delta \boldsymbol{q} + \boldsymbol{g}(\boldsymbol{q})$.

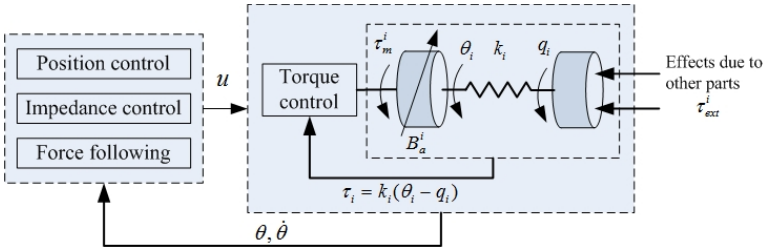

Fig. 7: Two-loop joint control scheme

Let mapping $T(\boldsymbol{q}) := \theta - K^{-1}\boldsymbol{h}(\boldsymbol{q})$. By Property 4.4, there is

$$\begin{aligned}\left\|\frac{\partial \boldsymbol{h}}{\partial \boldsymbol{q}}\right\| &= \left\|-K_q + \frac{\partial \boldsymbol{g}}{\partial \boldsymbol{q}}\right\| \le \|K_q\| + \left\|\frac{\partial \boldsymbol{g}}{\partial \boldsymbol{q}}\right\| \le \|K_q\| + k_g \\ &\le \gamma,\end{aligned}$$

where γ is some finite positive real number.

Moreover, assume that $\|K\| > \gamma$, *i.e.*, there exists an upper bound on the desired stiffness K_q. This is not surprising since the controller basically implements a stiffness, which is in cascade interconnection to the joint stiffness K. The stiffness K_q, therefore, must be smaller than K. We have

$$\begin{aligned}\|T(\boldsymbol{q}_1) - T(\boldsymbol{q}_2)\| &= \left\|K^{-1}(\boldsymbol{h}(\boldsymbol{q}_1) - \boldsymbol{h}(\boldsymbol{q}_2))\right\| \\ &\le \left\|K^{-1}\right\| \|(\boldsymbol{h}(\boldsymbol{q}_1) - \boldsymbol{h}(\boldsymbol{q}_2))\| \\ &\le \gamma\left\|K^{-1}\right\| \|\boldsymbol{q}_1 - \boldsymbol{q}_2)\| \\ &< \|\boldsymbol{q}_1 - \boldsymbol{q}_2)\|,\end{aligned}$$

i.e., the mapping $T(\boldsymbol{q})$ is a contraction. By the contraction mapping theorem [21], there is a unique fixed-point $\hat{\boldsymbol{q}}(\theta)$ such that $T(\hat{\boldsymbol{q}}(\theta)) = \hat{\boldsymbol{q}}(\theta)$.

To sum up, overall closed-loop system is rewritten as:

$$M(\boldsymbol{q})\ddot{\boldsymbol{q}} + C(\boldsymbol{q},\dot{\boldsymbol{q}})\dot{\boldsymbol{q}} + \boldsymbol{g}(\boldsymbol{q}) = \tau + \tau_{ext} \quad (13)$$

$$B_a\ddot{\theta} + D_q\dot{\theta} + \tau = \bar{\boldsymbol{h}}(\theta), \quad (14)$$

where $\bar{\boldsymbol{h}}(\theta) = \boldsymbol{h}(\hat{\boldsymbol{q}}(\theta)) = -K_q\delta\hat{\boldsymbol{q}}(\theta) + \boldsymbol{g}(\hat{\boldsymbol{q}}(\theta))$.

1) Passivity Analysis: A sufficient condition for a system (with input $\boldsymbol{u}$ and output $\boldsymbol{y}$) to be passive is that there exists a continuous storage function S, which is bounded from below and for which its Lie derivative satisfies the inequality $\dot{S} \le \boldsymbol{y}^T\boldsymbol{u}$ [22].

The passivity of (13) with respect to the input-output pair $\{\tau + \tau_{ext}, \dot{\boldsymbol{q}}\}$ is well known in terms of physical characteristics. This can also be shown by the storage function

$$S_{\boldsymbol{q}} = \frac{1}{2}\dot{\boldsymbol{q}}^T M(\boldsymbol{q})\dot{\boldsymbol{q}} + V_g(\boldsymbol{q}).$$

Using the second property of robot dynamical model, the Lie derivative is given by

$$\dot{S}_{\boldsymbol{q}} = \dot{\boldsymbol{q}}^T(\tau + \tau_{ext}).$$

In order to show the passivity of (14) with respect to the input-output pair $\{\dot{\boldsymbol{q}}, -\tau\}$, define the following storage function:

$$S_\theta = \frac{1}{2}\dot{\theta}^T B_a\dot{\theta} + \frac{1}{2}(\theta - \boldsymbol{q})^T K(\theta - \boldsymbol{q}) - V_{\bar{\boldsymbol{h}}}(\theta), \quad (15)$$

where $V_{\bar{\boldsymbol{h}}}(\theta)$ is a potential function for $\bar{\boldsymbol{h}}(\theta)$, satisfying $\bar{\boldsymbol{h}}(\theta) = (\partial V_{\bar{\boldsymbol{h}}}(\theta)/\partial\theta)^T$.

A potential function $V_{\boldsymbol{h}}(\hat{\boldsymbol{q}})$ in $\hat{\boldsymbol{q}}$ can readily be selected as:

$$V_{\boldsymbol{h}}(\hat{\boldsymbol{q}}) = -\frac{1}{2}\delta\hat{\boldsymbol{q}}^T K_q\delta\hat{\boldsymbol{q}} + V_{\boldsymbol{g}}(\hat{\boldsymbol{q}}). \quad (16)$$

As proven by [14], a potential function $V_{\bar{\boldsymbol{h}}}(\theta)$ in θ, satisfying $\bar{\boldsymbol{h}}(\theta) = (\partial V_{\bar{\boldsymbol{h}}}(\theta)/\partial\theta)^T$, can be defined as:

$$V_{\bar{\boldsymbol{h}}}(\theta) = V_{\boldsymbol{h}}(\hat{\boldsymbol{q}}(\theta)) + \frac{1}{2}\boldsymbol{h}^T(\hat{\boldsymbol{q}}(\theta))K^{-1}\boldsymbol{h}(\hat{\boldsymbol{q}}(\theta)). \quad (17)$$

$V_{\bar{\boldsymbol{h}}}(\theta)$ is bounded from below since all other terms are quadratic. In addition, the potential function $V_{\boldsymbol{g}}(\hat{\boldsymbol{q}})$ is upper bounded for robots with rotational joints only, i.e., there exists a real $\alpha > 0$, for any $\hat{\boldsymbol{q}} \in R^n$, such that $|\, V_{\boldsymbol{g}}(\hat{\boldsymbol{q}})\,| < \alpha$. Hence, $V_{\bar{\boldsymbol{h}}}(\theta)$ is qualified as an appropriate storage function. Its Lie derivative is given by:

$$\dot{S}_\theta = -\dot{\theta}^T D_q\dot{\theta} - \dot{\boldsymbol{q}}^T\tau \le -\dot{\boldsymbol{q}}^T\tau. \quad (18)$$

Thus the subsystem is strictly passive with respect to $\{\dot{\boldsymbol{q}}, -\tau\}$. Since the human body is considered to be passive during robot massage, the coupled stability is guaranteed as a parallel and feedback interconnection of two passive subsystems and passive environment [23].

It should be mentioned that the storage functions can be used as a Lyapunov function for proof of asymptotic stability in case of free motion ($\tau_{ext} = \boldsymbol{0}$) [14], [24]. Certainly, if contact dynamics is exactly known, it can also be the Lyapunov function in case of constraint motion.

V. Experimental Verification

A. Massage Force Measurement Device and Testbed

As shown in Fig. 8, a massage force measurement device is specifically designed to measure *in vivo* human expert's fingertip forces during massage therapies by FlexiForce, an ultra-thin, flexible piezoresistive force sensor manufactured by the Tekscan Incorporation. In our application, FlexiForce sensor is put between ceramic massage head and pressing bar avoiding the influence due to deformation of soft tissues. Hence therapist's fingertip forces are authentically measured without force transmission loss. Measurement data

are recorded by computer, from which massage force curves, massage movement frequencies, and massage time durations as well as massage rhythms are extracted.

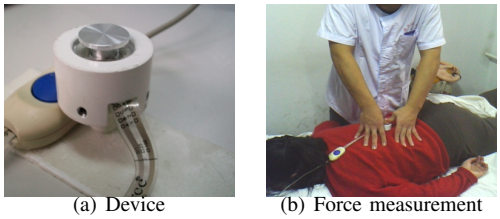

(a) Device (b) Force measurement

Fig. 8: Massage force measurement

A testbed in Fig. 9 is built to evaluate robot massage performance, which is composed of the 4-DOF anthropomorphic robotic arm, a massage bed, and a torso model. An array of FlexiForce sensors is adhered on the torso model whose locations represent the corresponding acupoints on the back, and is covered by a sheet of silicone polymer to simulate soft tissues.

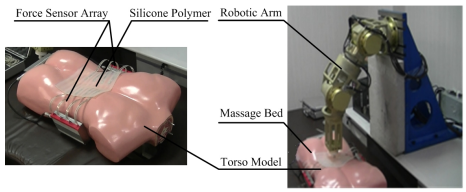

Fig. 9: Torso model and testbed used in experiments

B. Robot Massage on Torso Model and Users' Evaluation

1) Massage Force Following: During therapist's massage, force curve is recorded. When the robotic arm realizes massage manipulation on the torso model, it will be a reasonable judgement that robot massage can rival that of therapist if the time-force curve generated by the robotic arm is highly similar to that measured beforehand. Figure 10 shows that the robotic arm can replicated the recorded force curve within acceptable tolerance.

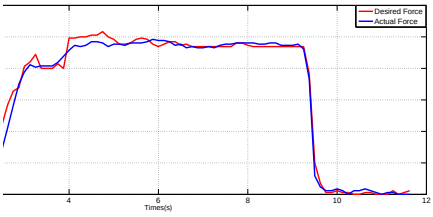

Fig. 10: Massage force curves by robotic arm and therapist

2) Pressing, Kneading and Plucking on Torso Model: Since contact dynamics between robotic arm and human body varies with different persons as well as each person's different contact parts, it can hardly be modeled appropriately in a meaningful way. Fortunately, we can adjust massage force in real-time according to users' reaction. The concrete implementation is as follows: Identify the upper and lower limits of massage force, and fuzzily partition into a number of value intervals, labeled as for example large, medium, and small. Once massage force falls into a given interval, it is realized with a fixed force value chosen from the interval or a force curve determined by some fuzzy rules. At the onset, massage force is roughly set, and then is tuned rapidly corresponding to users' reaction.

Motion and force in pressing have the same direction. In contrast, motion direction and force direction in kneading and plucking are approximately orthogonal, and massage head applies a vertically downward force on the human body, and meanwhile moves periodically on its surface. Assume that the maximum massage force is 100N and the minimum 0N. The value intervals corresponding to large, medium, and small massage forces, respectively, are given as follows: [45,100], [15,45], [5,15]. Pressing, kneading and plucking with large, medium and small massage force are implemented on torso model around one fixed point, respectively. The massage force curves shown in Fig. 11 are measured by JR3 6-DOF force-torque sensors 50M31.

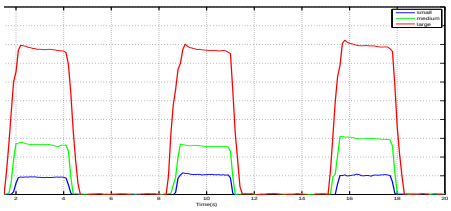

(a) Pressing

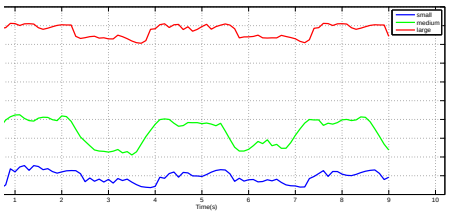

(b) Kneading

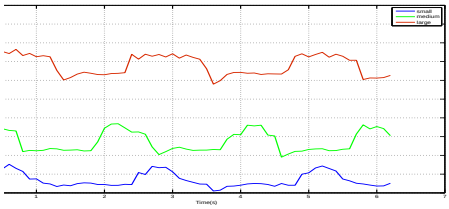

(c) Plucking

Fig. 11: Massage force curves by robotic arm

3) Users' Evaluation: Two scenarios with sitting and lying on massage bed in Fig. 12 are designed to evaluate

performance of robot massage. Robot massage is executed on 100 student volunteers with two postures. All of students are required to respond a questionnaire with questions related to satisfaction of robot massage and similarity between robot and human massages. Statistical analysis is presented in Table III.

TABLE III: Statistical analysis on questionnaire forms

Score	Satisfaction	Similarity
Excellent	11%	2%
Good	52%	41%
Medium	47%	54%
Bad	0%	3%

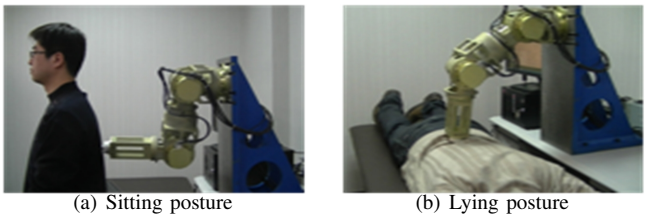

(a) Sitting posture (b) Lying posture

Fig. 12: Two scenarios for users' evaluation

VI. Conclusions and Further Works

In this paper, integrated elastic joint is designed by taking both performance and safety into consideration. Due to series elasticity, low impedance can effectively decouple the link's inertia from the actuator's reflected inertia whenever impact occurs, and more accurate and stable force control and a capacity for energy storage can be offered. Using the integrated elastic joints, a 4-DOF compact anthropomorphic robotic arm for three massage techniques is developed with characteristics of compactness, light weight, and safety, and a passivity-based impedance control with inner torque loop is conceived for both free and constraint motions in robot massage. Then, a proprietary massage force measurement device is designed to acquire human expert's fingertip force curve *in vivo*, and a testbed is built to verify the performance of robot massage. Experimental results and users' evaluation demonstrate that the developed robotic arm can replicate the therapist's massage techniques with good quality and high safety.

To conclude, our goals at initial stage are achieved successfully. But we fail to build a 7-DOF anthropomorphic robotic arm by the current integrated elastic joints due to its heavy weight. In the next stage, a 3-DOF compact, lightweight, and small-size differential wrist will be designed by using rigid joints, and thus a 7-DOF anthropomorphic robotic arm with the wrist will be developed for the massage techniques with wrist movement. It is taken for granted to study further the passivity-based impedance control of redundant robotic arm mingled with both compliant and rigid joints.

VII. Acknowledgments

The authors gratefully appreciate the support of this research by the National Natural Sciences Foundation of China and by the Minister of Science and Technology of China, and anonymous reviewers' comments.

References

[1] M. Kume, *et al*., Development of a Mechanotherapy Unit for Examining the Possibility of an Intelligent Massage Robot, *Proc. of IEEE/RSJ Int. Conf. on Intelligent Robots and Systems*, Osaka, pp.346-353, 1996.

[2] K.C. Jones and D. Winncy, Development of a Massage Robot for Medical Therapy, *Proc. of IEEE/ASME Int. Conf. on Advanced Intelligent Mechatronics*, pp.1096-1101, 2003.

[3] H. Koga, *et al*., Development of Oral Rehabilitation Robot for Massage Therapy, *Proc. of Int. Special Topic Conf. on ITAB*, Tokyo, pp.111-114, 2007.

[4] M. Grebenstein, *et al.*, The DLR Hand Arm System, *Proc. IEEE/RSJ Int. Conf. Intelligent Robots and Systems*, Shanghai, pp.3175-3128, 2011.

[5] N. G. Tsagarakis, *et al.*, iCub CThe Design and Realization of an Open Humanoid Platform for Cognitive and Neuroscience Research, *Advanced Robotics*, Vol.21, No.10, pp. 1151-1175, 2007.

[6] Y.C. Huang, *et al.*, Integrated Rotary Compliant Joint and Its Impedance-based Controller for Single-Joint Pressing Massage Robot, *Proc. IEEE Int. Conf. Robotics and Biomimetics*, Guangzhou, pp. 1962-1967, 2012.

[7] E. I. Rivin, Mechanical Design of Robots. New York: McGraw-Hill Book Company, 1988.

[8] http://mekabot.com/products/compliant-arm/.

[9] http://www.ai.mit.edu/projects/humanoid-robotics-group/cog/.

[10] G. A. Pratt and M. Williamson, Series elastic actuators, *Proc. IEEE/RSJ Int. Conf. Intell. Robot. Syst.*, Pittsburgh, PA, pp. 399-406, 1995.

[11] J. Pratt, B. Krupp, and C. Morse, Series Elastic Actuators for High Fidelity Force Control, *Int. J. Ind. Robot*, vol. 29, no. 3, pp. 234-241, 2002.

[12] D. W. Robinson, J. E. Pratt, D. J. Paluska, and G. A. Pratt, Series Elastic Actuator Development for a Biomimetic Walking Robot, *Proc. IEEE/ASME Int. Conf. Adv. Intell. Mech.*, Atlanta, GA, pp. 561-568, 1999.

[13] A. Albu-Schäffer, C. Ott, and G. Hirzinger, A Unified Passivity-based Control Framework for Position, Torque and Impedance Control of Flexible Joint, *Int. J. Robot. Res.*, vol. 26, no. 1, pp. 23-39, 2007.

[14] C. Ott, *et al.*, On the Passivity-Based Impedance Control of Flexible Joint Robots, *IEEE J. Robotics Auromat.*, VOL. 24, NO. 2, pp. 416-429, 2008.

[15] M. W. Spong, Modeling and Control of Elastic Joint Robots, *ASME J. Dynam. Syst. Meas. Contr.*, vol. 109, pp. 310-319, 1987.

[16] R. Gunawardana and F. Ghorbel, The Class of robot Manipulators With Bounded Jacobian of the Gravity Vector, *in Proc. IEEE Int. Conf. Robotics and Automation*, Minneapolis, pp. 3677-3682, 1996.

[17] N. Hogan, Impedance Control: An Approach to Manipulation, Part I-Theory, Part II-Implementation, Part III-Applications, *ASME Journal of Dynamic Systems, Measurement and Control*, vol. 107, no. 3, pp. 1-24, 1985.

[18] C. Otta, A. Albu-Schäffer, and G. Hirzinger, A Passivity-based Cartesian Impedance Controller for Flexible Joint Robots-Part I: Torque Feedback and Gravity Compensation, *Proc. IEEE Int. Conf. on Robotics and Automation*, pp. 2659-2665, 2004.

[19] A. Albu-Schäffer, C. Otta, and G. Hirzinger, A Passivity-based Cartesian Impedance Controller for Flexible Joint Robots-Part II: Full State Feedback, Impedance Design and Experiments, *Proc. IEEE Int. Conf. on Robotics and Automation*, pp. 2666-2673, 2004.

[20] L. Zollo, *et al*., Compliance Control for an Anthropomorphic Robot with Elastic Joints: Theroy and Experiments, *ASME Journal of Dynamic Systems, Measurement and Control*, vol. 127, no. 3, pp. 321-328, 2005.

[21] M. Vidyasagar, Nonlinear Systems Analysis. Prentice-Hall, 1978.

[22] A. van der Schaft, L2-Gain and Passivity Techniques in Nonlinear Control, 2nd ed. New York: Springer-Verlag, 2000.

[23] J. Won and N. Hogan, Coupled Stability of Non-nodic Physical Systems, *IFAC Nonlinear Control Systems Design*, Enschede, The Netherlands, pp. 573-578, 1998.

[24] A. Albu-Schäffer, Ott, C. and Hirzinger, G. Passivity Based Cartesian Impedance Control for Flexible Joint Manipulators. *6th IFAC Symposium on Nonlinear Control Systems*, Vol. 2, pp. 1175-1180, 2004.